LETTER

doi:10.1038/nature10903

Spontaneous coherence in a cold exciton gas

A. A. High[1], J. R. Leonard[1], A. T. Hammack[1], M. M. Fogler[1], L. V. Butov[1], A. V. Kavokin[2,3], K. L. Campman[4] & A. C. Gossard[4]

If bosonic particles are cooled down below the temperature of quantum degeneracy, they can spontaneously form a coherent state in which individual matter waves synchronize and combine. Spontaneous coherence of matter waves forms the basis of a number of fundamental phenomena in physics, including superconductivity, superfluidity and Bose–Einstein condensation[1,2]. Spontaneous coherence is the key characteristic of condensation in momentum space[3]. Excitons—bound pairs of electrons and holes—form a model system to explore the quantum physics of cold bosons in solids[4,5]. Cold exciton gases can be realized in a system of indirect excitons, which can cool down below the temperature of quantum degeneracy owing to their long lifetimes[6]. Here we report measurements of spontaneous coherence in a gas of indirect excitons. We found that spontaneous coherence of excitons emerges in the region of the macroscopically ordered exciton state[7] and in the region of vortices of linear polarization. The coherence length in these regions is much larger than in a classical gas, indicating a coherent state with a much narrower than classical exciton distribution in momentum space, characteristic of a condensate. A pattern of extended spontaneous coherence is correlated with a pattern of spontaneous polarization, revealing the properties of a multicomponent coherent state. We also observed phase singularities in the coherent exciton gas. All these phenomena emerge when the exciton gas is cooled below a few kelvin.

There are intriguing theoretical predictions for a range of coherent states in cold exciton systems, including the Bose–Einstein condensate[4], a BCS-like condensate[5], the charge-density wave[8], and a condensate with spontaneous time-reversal symmetry breaking[9]. Because excitons are much lighter than atoms, quantum degeneracy can be achieved in excitonic systems at temperatures orders of magnitude higher than the microkelvin temperatures needed in atomic vapours[1,2]. Exciton gases need be cooled down to a few kelvin to enter the quantum regime. Although the temperature of the semiconductor crystal lattice (T_l) can be lowered well below 1 K in helium refrigerators, lowering the temperature of the exciton gas (T_X) to even a few kelvin is challenging[10,11]. Owing to recombination, excitons have a finite lifetime that is too short to allow cooling to low temperatures in usual semiconductors. In order to create a cold exciton gas with T_X close to T_l, the exciton lifetime should considerably exceed the exciton cooling time. As well as this, the realization of a cold and dense exciton gas requires an excitonic state to be the ground state and to have lower energy than the electron–hole liquid[12].

A gas of indirect excitons fulfils these requirements. An indirect exciton can be formed by an electron and a hole confined in separate quantum-well layers (Fig. 1a, b). The spatial separation allows the overlap of electron and hole wavefunctions to be controlled. In this way, indirect excitons can be produced with radiative lifetimes and spin relaxation times orders of magnitude longer than those of direct excitons[13–15].

In earlier studies, evidence for spontaneous coherence was obtained for indirect excitons in coupled quantum wells (CQWs)[16] and for indirect excitons in quantum Hall bilayers[17,18]. The onset of spontaneous coherence was evidenced by a strong enhancement of the rates of recombination[16] and tunnelling[17], respectively. The results of other transport and optical experiments were also consistent with spontaneous coherence of indirect excitons[6,16–22]. However, no direct measurement of coherence was performed in these studies.

Exciton coherence is evidenced by coherence of their light emission, which can be studied by interferometry. In our earlier work, we reported an enhancement of the exciton coherence length in the macroscopically ordered exciton state[23,24] (MOES). However, these experiments used a single-pinhole interferometric technique, which does not measure the coherence function, and the derivation of the exciton coherence length in refs 23 and 24 was based on a mathematical analysis of the data.

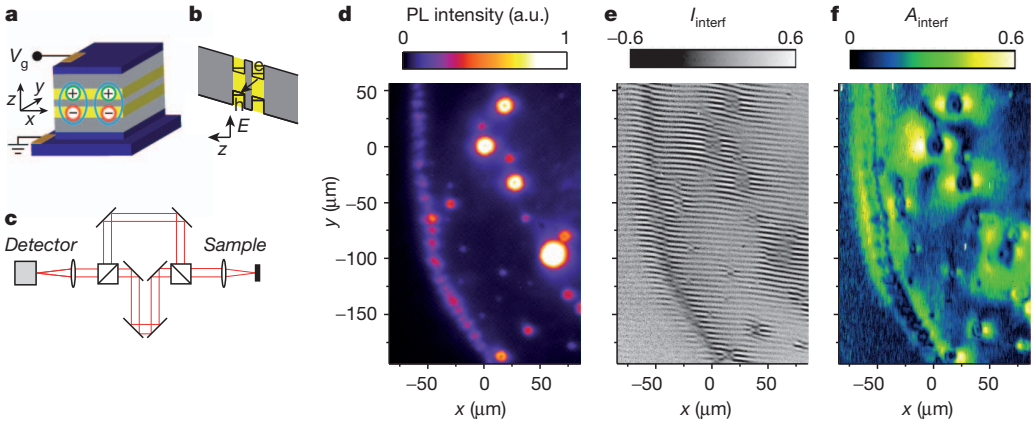

Figure 1 | Emission, interference and coherence patterns of indirect excitons. **a**, Diagram of CQW structure: n^+-GaAs (blue), $Al_{0.33}Ga_{0.67}As$ (grey), GaAs quantum well (yellow). V_g is applied voltage. Ellipses indicate indirect excitons composed of electrons (–) and holes (+). **b**, CQW band diagram; e, electron; h, hole; E, energy. The arrow indicates an indirect exciton. **c**, Diagram of the interferometric set-up. **d**, Emission pattern (luminescence). **e**, Interference pattern $I_{interf}(x, y)$ for $\delta x = 2$ μm. **f**, Pattern of the amplitude of the interference fringes $A_{interf}(x, y)$, presenting a map of coherence. The temperature in the refrigerator at the sample is $T_{bath} = 0.1$ K.

[1]Department of Physics, University of California at San Diego, La Jolla, California 92093-0319, USA. [2]School of Physics and Astronomy, University of Southampton, Southampton SO17 1BJ, UK. [3]Spin Optics Laboratory, State University of Saint Petersburg, 1, Ulianovskaya, 198504, Russia. [4]Materials Department, University of California at Santa Barbara, Santa Barbara, California 93106-5050, USA.

Here we report the direct measurement of spontaneous coherence in a gas of indirect excitons in CQWs. These indirect excitons may have four spin projections on the z direction normal to the CQW plane: $J_z = -2, -1, +1, +2$. The states $J_z = -1$ and $+1$ contribute to left- and right-circularly polarized emission and their coherent superposition to linear polarized emission, whereas the states $J_z = -2$ and $+2$ are dark[9,15]. The exciton condensate is a four-component coherent state in general. The build-up of exciton coherence should manifest itself in an increase of the coherence length and of the degree of polarization of the exciton emission. The former phenomenon is general for both one- and multicomponent condensates[3], whereas the latter is specific to multi-component condensates[25]. In this work, we report the emergence of both long-range spontaneous coherence of excitons and spontaneous polarization. A pattern of extended spontaneous coherence, measured by shift interferometry (see below), is correlated with a pattern of spontaneous polarization, measured by polarization-resolved imaging. These two experiments reveal the properties of a multi-component coherent state.

The pattern of the first-order coherence function $g_1(\delta x)$ is measured by shift interferometry: the emission images produced by each of the two arms of the Mach–Zehnder interferometer (Fig. 1c) are shifted with respect to each other to measure the interference between the emission of excitons spatially separated by δx. Details of the experiment are given in Supplementary Information.

Extended spontaneous coherence is observed in the region of rings in the exciton emission pattern. Exciton rings—including the inner ring, external ring and localized bright spot (LBS) rings—were observed earlier[7]. The external and LBS rings form on the boundaries between electron-rich and hole-rich regions; the former is created by current through the structure (specifically, by the current filament at the LBS centre in the case of the LBS ring), whereas the latter is created by optical excitation[26,27]. The external and LBS rings are sources of cold excitons. In the area of these rings coherence forms spontaneously. Figure 1d shows a segment of the exciton emission pattern, with a section of the external ring and smaller LBS rings.

The pattern of interference fringes is shown in Fig. 1e and the map of their amplitude, A_{interf}, in Fig. 1f. The quantity A_{interf} describes the degree of coherence of excitons, as detailed below. The regions of extended spontaneous coherence of excitons correspond to the green colour in Fig. 1f.

Figure 2 presents the patterns of coherence of emission from indirect excitons in regions of an LBS and the external ring. The observed properties of exciton coherence are qualitatively similar around both these sources of cold excitons. We first consider an LBS region. At low temperatures, a strong enhancement of A_{interf} is observed at distance $r \approx r_0 = 7\,\mu\mathrm{m}$ away from the LBS centre (Fig. 2b, c, i). This enhancement of the degree of coherence shows the emergence of extended spontaneous coherence of excitons.

Furthermore, the phase of the interference fringes, ϕ_{interf}, experiences a shift at $r \approx r_0 = 7\,\mu\mathrm{m}$, which defines a phase domain boundary (Fig. 2b). The shift in phase correlates with the enhancement of A_{interf} (Fig. 2b, c). Its magnitude $\delta\varphi = \varphi_{\mathrm{interf}}^{\mathrm{outer}} - \varphi_{\mathrm{interf}}^{\mathrm{inner}}$ increases with δx (Fig. 2j). The interference pattern in the shift-interferometry experiment with shift δx can be simulated using the formula $I_{\mathrm{interf}} = |\Psi(\mathrm{r}) + \mathrm{e}^{iq_{\mathrm{t}}y}\Psi(\mathrm{r}+\delta\mathrm{x})|^2$, where $q_{\mathrm{t}} = 2\pi\alpha/\lambda$ sets the period of interference fringes (α is a small tilt angle between the image planes of the interferometer arms, λ is the emission wavelength) and the complex function $\Psi(\mathbf{r})$ represents the source amplitude at point $\mathbf{r}$. For a flow of excitons with momentum $\mathbf{q}$, $\Psi(\mathbf{r}) = \mathrm{e}^{i\mathbf{qr}}$, so that $I_{\mathrm{interf}} = 2 + 2\cos(q_{\mathrm{t}}y + \mathbf{q}\delta\mathbf{x})$ and the shift in the phase of the interference fringes means a jump in (average) measured exciton momentum $\delta q \approx \delta\phi_{\mathrm{interf}}/\delta x \approx 2\,\mu\mathrm{m}^{-1}$ at $r = r_0$.

Figure 2d presents a pattern of linear polarization around an LBS. It spatially correlates with the pattern of the amplitude and phase of the interference fringes: compare Fig. 2b, c and d. At $r \gtrsim r_0$ a vortex of linear polarization with the polarization perpendicular to the radial direction is observed. Such polarization vortices appear owing to precession of the Stokes vector for excitons propagating out of the LBS origin (see Supplementary Information for details).

To summarize, close to the heating sources within the LBS ring the exciton gas is hot, and no spontaneous coherence forms there (the heating of the exciton gas is due to the current filament at the LBS centre and the binding energy released at the exciton formation in the ring[26]). This is revealed by the small amplitude of the interference fringes. Excitons cool down with increasing distance r away from the heating sources so that they can approach the transition temperature to a coherent state. At $r = r_0$, the (average) exciton momentum reduces and the coherence degree sharply rises, indicating the emergence of extended spontaneous coherence of excitons. This is revealed by the shift in the phase of the interference fringes and the strong enhancement of the amplitude of the interference fringes, respectively. The polarization vortex emerges along with extended spontaneous coherence at $r = r_0$, revealing the properties of a multicomponent coherent state.

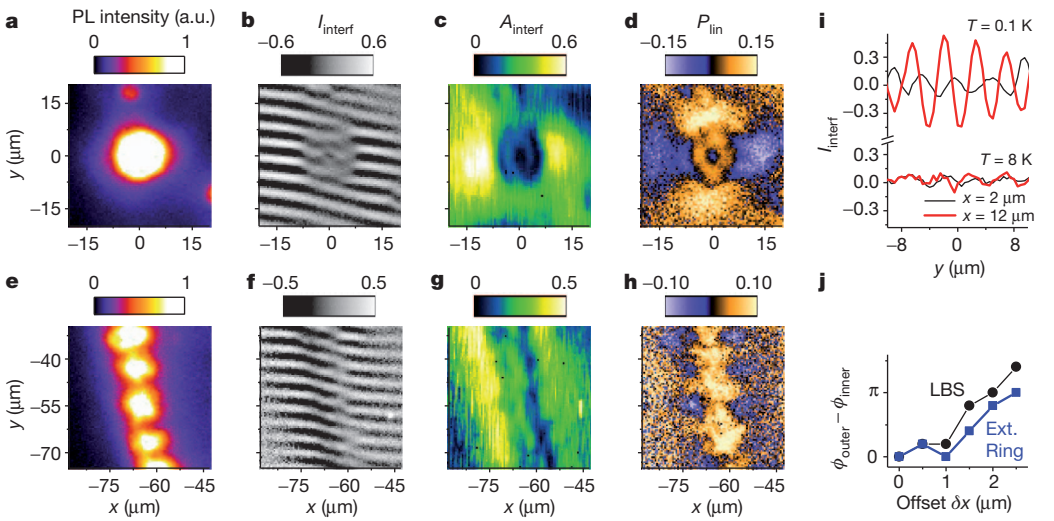

Figure 2 | Coherence of indirect excitons in regions of an LBS and the external ring. **a**–**d**, A region of an LBS; **e**–**h**, a region of the external ring. Shown are the emission pattern (**a**, **e**), the interference pattern at shift $\delta x = 2\,\mu\mathrm{m}$ (**b**, **f**), the amplitude $A_{\mathrm{interf}}(x, y)$ of interference fringes (**c**, **g**), and the linear polarization of exciton emission $P_{\mathrm{lin}} = (I_x - I_y)/(I_x + I_y)$ (**d**, **h**). **i**, y-axis cross-sections of $I_{\mathrm{interf}}(x, y)$ at $x = 2\,\mu\mathrm{m}$ (black lines) and $x = 12\,\mu\mathrm{m}$ (red lines) at $T_{\mathrm{bath}} = 0.1$ K and 8 K. **j**, The shift in the phase of interference fringes in **b** at $r \approx 7\,\mu\mathrm{m}$ (black) and in **f** at $\sim 4\,\mu\mathrm{m}$ away from the centre of the external ring (blue) versus δx. $T_{\mathrm{bath}} = 0.1$ K for **a**–**h**, **j**.

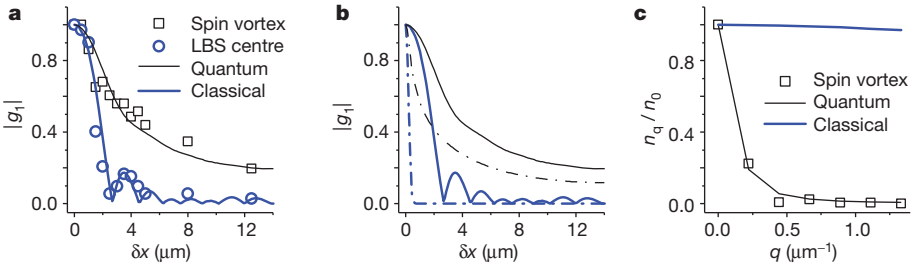

Figure 3 | First-order coherence function and distribution in momentum space. **a**, Measured $|g_1(\delta x)|$ for the polarization vortex (squares) and LBS centre (circles), and simulated $|g_1(\delta x)|$ for a quantum (black line) and classical (blue line) gas. **b**, Simulated $|g_1(\delta x)|$ for a quantum (black) and classical (blue) gas with (solid) and without (dashed) convolution with the PSF. **c**, Distribution in momentum space obtained by the Fourier transform of g_1 in **b** for a quantum (black line) and a classical (blue line) gas. See main text for details.

Similar phenomena are observed in the external ring region. At low temperature, the MOES forms in the external ring[7] (Figs 1d and 2e) and a periodic polarization texture forms around the periodic array of beads in the MOES (Fig. 2h). Figure 2f and g shows the extended spontaneous coherence of excitons observed in the MOES. It emerges at low temperatures, along with the spatial order of exciton beads and periodic polarization texture.

We now discuss the measurements of the first-order coherence function. Coherence of the exciton gas is directly characterized by coherence of exciton emission, described by the first-order coherence function $g_1(\delta\mathbf{r})$. In turn, this function is given by the amplitude of the interference fringes $A_{\text{interf}}(\delta\mathbf{r})$ in 'the ideal experiment' with perfect spatial resolution. In practice, the measured $A_{\text{interf}}(\delta\mathbf{r})$ is given by the convolution of $g_1(\delta\mathbf{r})$ with the point-spread function (PSF) of the optical system used in the experiment[24]. The PSF width corresponds to the spatial resolution of the optical system (~1.5 μm in our experiments).

The measurements of $A_{\text{interf}}(\delta x)$ in the polarization vortex and in the LBS centre are presented in Fig. 3a. In the hot LBS centre, A_{interf} quickly drops with δx and the shape $A_{\text{interf}}(\delta x)$ fits well to the PSF, which is shown by the blue line. In the polarization vortex, $g_1(\delta x)$ extends to large δx, demonstrating extended spontaneous coherence. A fit to the experimental points computed using a model described below is shown by the black line (Fig. 3a).

Figure 3b and c demonstrates the relation between the first-order coherence function and the particle distribution in momentum space. Figure 3b presents $g_1(\delta x)$ for a classical gas (blue dashed line) and for a quantum gas (black dashed line); both curves are for a spatially homogeneous gas of non-interacting particles with a quadratic dispersion (see Supplementary Information). Both gases are at 0.1 K; the occupation number of the $q = 0$ momentum state (n_0) is $\ll 1$ for the classical gas, but is 5,000 for the quantum gas. The convolution of these $g_1(\delta x)$ with the PSF produces data shown as black and blue solid lines, which fit to $A_{\text{interf}}(\delta x)$ in the spin polarization vortex and in the LBS centre, respectively (Fig. 3a, b). The Fourier transform of $g_1(\delta x)$ in Fig. 3b gives the momentum occupation factor n_q shown in Fig. 3c.

Figure 3b and c illustrates that a classical gas is characterized by a broad distribution in momentum space n_q and a narrow first-order coherence function $g_1(r)$, whereas a quantum gas is characterized by a narrow n_q and an extended $g_1(r)$. For a classical gas, $g_1(r)$ reduces substantially within the thermal de Broglie wavelength λ_{dB}, which scales $\propto T^{-1/2}$ and is about 0.5 μm at 0.1 K. The extension of $g_1(r)$ well beyond λ_{dB} indicates a coherent exciton state.

Figure 3a also illustrates why $\delta x = 2$ μm is selected for mapping extended spontaneous coherence of excitons. The shift $\delta x = 2$ μm is chosen to exceed both λ_{dB} and the PSF width. At such δx, only weak coherence given by the PSF value at $\delta x = 2$ μm can be observed for a classical gas. The regions of enhanced coherence exceeding such a background level reveal the regions with extended spontaneous coherence of excitons.

Next, we present a pattern of coherence length. The spatial extension of $g_1(\delta r)$ can be characterized by a coherence length ξ. To consider all the points in the pattern on an equal footing, we evaluate ξ as that value of δr at which the interference visibility drops e times. We measured the exciton interference pattern at different δr to produce the spatial map of $g_1(\delta r)$ and, in turn, ξ. Figure 4a and b shows the pattern of ξ for the shift between the interfering excitons along x and y, respectively. Figure 4c and d presents the cross-sections of $\xi(x, y)$ in the region of the polarization vortex (Fig. 4c) and MOES (Fig. 4d).

The regions of a classical gas in the $\xi(x, y)$ pattern correspond to the smallest observed coherence length, which is given by the PSF width. Long-range spontaneous coherence of excitons is observed in the polarization vortices and in the macroscopically ordered exciton state (Fig. 4). The coherence length in these regions is much larger than in a classical gas, indicating a coherent state with a much narrower-than-classical exciton distribution in momentum space, characteristic of a condensate.

The observed coherence length in the polarization vortex exceeds $\lambda_{\text{dB}} = 0.5$ μm at 0.1 K by more than an order of magnitude (Fig. 4). The coherence length in the MOES is smaller than in the polarization vortex. This may be related to fluctuations of the exciton density wave in the external ring. Such fluctuations were observed recently, and their studies will be reported in future work.

The patterns of coherence length are different for the shifts along x and y, revealing a directional property of exciton coherence. In the

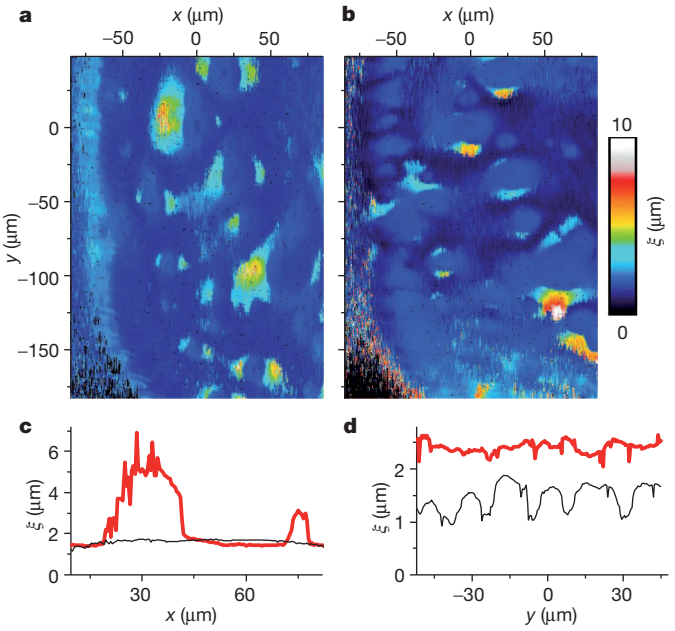

Figure 4 | Patterns of the coherence length of excitons, $\xi(x, y)$. **a**, **b**, $\xi(x, y)$ for a shift along x (**a**) and y (b). **c**, **d**, Cross-section of $\xi(x, y)$ through LBS ($y = -90$ μm; **c**) and along the external ring ($x = -70$ μm; **d**) for a shift along x (red) and y (black). $T_{\text{bath}} = 0.1$ K.

region of the polarization vortices, ξ is higher in the direction along the shift between the interfering excitons (that is, the x direction for the δx shift (Fig. 4a), and the y direction for the δy shift (Fig. 4b)). In the region of the MOES, ξ is higher for the δx shift (that is, for the shift along the direction of exciton propagation away from the external ring in Fig. 4a). These data indicate that the extension of $g_1(\mathbf{r})$ is greater when the exciton propagation direction is along vector $\mathbf{r}$.

Finally, we present observations of phase singularities. A well known example of a phase singularity is a quantized vortex. In a singly quantized vortex, the phase of the wavefunction winds by 2π around the singularity point, which can be revealed as a fork-like defect in a phase pattern. Fork-like defects in interference patterns have been reported for optical vortices, vortices in atom condensates, and polariton vortices (see refs 28–30 and references therein).

We observed a number of fork-like defects in the interference pattern of a cold exciton gas. For example, more than 20 such defects are present in Fig. 1e. Information on an enlarged scale is presented in Fig. 5. Figure 5a shows forks in the interference pattern, indicating the presence of phase singularities. We have studied the properties of this phenomenon and show below that its origin is different from that of a quantized vortex.

The forks in the interference pattern are observed at low temperatures in a quantum exciton gas (Fig. 5a) and vanish at high temperatures in a classical exciton gas (Fig. 5d). At low temperatures, a closed contour around the fork crosses an odd number of interference fringes, so the phase of the interference fringes winds by 2π, indicating a phase singularity (Fig. 5e). Similar properties are observed for quantized vortices.

However, the distance between the left- and right-facing forks in the interference pattern is different from the shift $\delta x = 2\,\mu$m in the shift-interferometry experiment, and depends on the excitation power (Fig. 5a–c). This indicates the difference between the observed phase singularity and a quantized vortex. Indeed, straightforward simulations show that a quantized vortex is characterized by a pair of opposite forks separated by a distance equal to the shift in the shift-interferometry experiment (see Supplementary Information).

Simulations of the interference pattern produced by a ring-shaped source, such as an LBS ring, result in an interference pattern with opposite forks separated by a distance much larger than δx, in qualitative agreement with the experiment (see Supplementary Information).

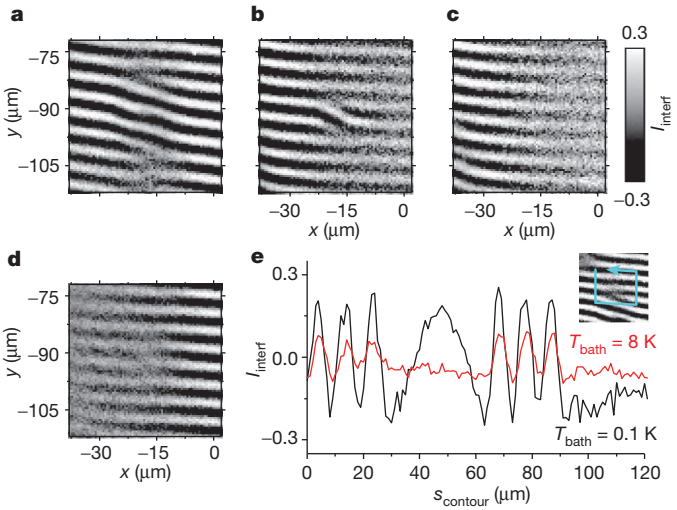

Figure 5 | Fork-like defects in exciton interference patterns. **a**–**d**, Interference pattern $I_{interf}(x, y)$ around an LBS; for **a**–**c**, T_{bath} is constant (0.1 K) and P_{ex} varies (7, 1.2 and 0.7 mW, respectively); for **a** and **d**, P_{ex} is constant (7 mW) and T_{bath} varies (0.1 and 5 K, respectively). **e**, I_{interf} along a closed contour (shown in inset) for $T_{bath} = 0.1$ K (black) and 8 K (red). $\delta x = 2\,\mu$m.

A ring-shaped source with particles propagating away from their origin on the ring produces a more complicated phase pattern than a vortex, yet both objects are characterized by the spreading of particle velocities over all directions. The observed phase singularities constitute the properties of a quantum exciton gas with extended spontaneous coherence (Fig. 5a), and no such phase singularity is observed at high temperatures in a classical gas (Fig. 5d).

METHODS SUMMARY

Experiments are performed on a n^+-i-n^+ GaAs/AlGaAs CQW structure. The i region consists of a single pair of 8-nm GaAs quantum wells separated by a 4-nm $Al_{0.33}Ga_{0.67}As$ barrier and surrounded by 200-nm $Al_{0.33}Ga_{0.67}As$ barrier layers. The n^+ layers are Si-doped GaAs with Si concentration $N_{Si} = 5 \times 10^{17}\,cm^{-3}$. The electric field in the z direction is controlled by the external voltage applied between n^+ layers. The small in-plane disorder in the CQW is indicated by the emission linewidth of 1 meV. Long lifetimes of the indirect excitons allow them to cool to temperatures within about 0.1 K of the lattice temperature, which can be lowered to 0.1 K in an optical dilution refrigerator. This allows the realization of a cold exciton gas with temperature well below the temperature of quantum degeneracy, which is in the range of a few kelvin for typical exciton densities $\sim 10^{10}\,cm^{-2}$ for the CQW[6]. The laser excitation is performed by a HeNe laser at excitation wavelength $\lambda_{ex} = 633$ nm with an excitation power $P_{ex} = 1.2$ (2.9) mW for the data in Figs 1–3 (Fig. 4). The photoexcitation is more than 400 meV above the energy of indirect excitons, and the 10-μm-wide excitation spot is farther than 80 μm away from both the LBS and the external ring. The x-polarization is along the sample cleavage direction within the experimental accuracy. The data have been acquired on a timescale of the order of 100 s. During the measurements, the LBS rings are static while the exciton density wave in the external ring fluctuates on a length scale of few micrometres (such fluctuations may be responsible for a smaller coherence length in the MOES than in the polarization vortex, as discussed in the text). The coherence length is generally smaller than the distance between the LBS and MOES, or between different LBS. The spatial resolution of the optical system is $\sim 1.5\,\mu$m.

Received 9 September 2011; accepted 17 January 2012.
Published online 21 March 2012.

1. Cornell, E. A. & Wieman, C. E. Bose-Einstein condensation in a dilute gas, the first 70 years and some recent experiments. *Rev. Mod. Phys.* **74,** 875–893 (2002).
2. Ketterle, W. When atoms behave as waves: Bose-Einstein condensation and the atom laser. *Rev. Mod. Phys.* **74,** 1131–1151 (2002).
3. Penrose, O. & Onsager, L. Bose-Einstein condensation and liquid helium. *Phys. Rev.* **104,** 576–584 (1956).
4. Keldysh, L. V. & Kozlov, A. N. Collective properties of excitons in semiconductors. *Sov. Phys. JETP* **27,** 521–528 (1968).
5. Keldysh, L. V. & Kopaev, YuV Possible instability of the semimetallic state toward Coulomb interaction. *Sov. Phys. Solid State* **6,** 2219–2224 (1965).
6. Butov, L. V. *et al.* Stimulated scattering of indirect excitons in coupled quantum wells: signature of a degenerate Bose-gas of excitons. *Phys. Rev. Lett.* **86,** 5608–5611 (2001).
7. Butov, L. V., Gossard, A. C. & Chemla, D. S. Macroscopically ordered state in an exciton system. *Nature* **418,** 751–754 (2002).
8. Chen, X. M. & Quinn, J. J. Excitonic charge-density-wave instability of spatially separated electron-hole layers in strong magnetic fields. *Phys. Rev. Lett.* **67,** 895–898 (1991).
9. Wu, C., Shem, I. M. & Exciton condensation with spontaneous time-reversal symmetry breaking.. Preprint at http://arXiv.org/abs/0809.3532v1 (2008).
10. Tikhodeev, S. G., Kopelevich, G. A. & Gippius, N. A. Exciton transport in Cu_2O: phonon wind versus superfluidity. *Phys. Status Solidi B* **206,** 45–53 (1998).
11. Jang, J. I. & Wolfe, J. P. Auger recombination and biexcitons in Cu_2O: a case for dark exciton matter. *Phys. Rev. B* **74,** 045211 (2006).
12. Keldysh, L. V. The electron-hole liquid in semiconductors. *Contemp. Phys.* **27,** 395–428 (1986).
13. Lozovik, YuE & Yudson, V. I. A new mechanism for superconductivity: pairing between spatially separated electrons and holes. *Sov. Phys. JETP* **44,** 389–397 (1976).
14. Fukuzawa, T., Kano, S. S., Gustafson, T. K. & Ogawa, T. Possibility of coherent-light emission from Bose condensed states of SEHPs. *Surf. Sci.* **228,** 482–485 (1990).
15. Maialle, M. Z., de Andrada e Silva, E. A. & Sham, L. J. Exciton spin dynamics in quantum wells. *Phys. Rev. B* **47,** 15776–15788 (1993).
16. Butov, L. V. & Filin, A. I. Anomalous transport and luminescence of indirect excitons in AlAs/GaAs coupled quantum wells as evidence for exciton condensation. *Phys. Rev. B* **58,** 1980–2000 (1998).
17. Spielman, I. B., Eisenstein, J. P., Pfeiffer, L. N. & West, K. W. Resonantly enhanced tunneling in a double layer quantum Hall ferromagnet. *Phys. Rev. Lett.* **84,** 5808–5811 (2000).
18. Eisenstein, J. P. & MacDonald, A. H. Bose-Einstein condensation of excitons in bilayer electron systems. *Nature* **432,** 691–694 (2004).

19. Butov, L. V., Zrenner, A., Abstreiter, G., Böhm, G. & Weimann, G. Condensation of indirect excitons in coupled AlAs/GaAs quantum wells. *Phys. Rev. Lett.* **73,** 304–307 (1994).
20. Tutuc, E., Shayegan, M. & Huse, D. A. Counterflow measurements in strongly correlated GaAs hole bilayers: evidence for electron-hole pairing. *Phys. Rev. Lett.* **93,** 036802 (2004).
21. Tiemann, L. *et al.* Exciton condensate at a total filling factor of one in Corbino two-dimensional electron bilayers. *Phys. Rev. B* **77,** 033306 (2008).
22. Karmakar, B., Pellegrini, V., Pinczuk, A., Pfeiffer, L. N. & West, K. W. First-order quantum phase transition of excitons in quantum hall bilayers. *Phys. Rev. Lett.* **102,** 036802 (2009).
23. Sen. Yang, Hammack, A. T., Fogler, M. M., Butov, L. V. & Gossard, A. C. Coherence length of cold exciton gases in coupled quantum wells. *Phys. Rev. Lett.* **97,** 187402 (2006).
24. Fogler, M. M. Sen Yang, Hammack, A. T., Butov, L. V. & Gossard, A. C. Effect of spatial resolution on the estimates of the coherence length of excitons in quantum wells. *Phys. Rev. B* **78,** 035411 (2008).
25. Read, D., Liew, T. C. H., Rubo, Y. G. & Kavokin, A. V. Stochastic polarization formation in exciton-polariton Bose-Einstein condensates. *Phys. Rev. B* **80,** 195309 (2009).
26. Butov, L. V. *et al.* Formation mechanism and low temperature instability of exciton rings. *Phys. Rev. Lett.* **92,** 117404 (2004).
27. Rapaport, R. *et al.* Charge separation of dense two dimensional electron-hole gases: mechanism for exciton ring pattern formation. *Phys. Rev. Lett.* **92,** 117405 (2004).
28. Scheuer, J. & Orenstein, M. Optical vortices crystals: spontaneous generation in nonlinear semiconductor microcavities. *Science* **285,** 230–233 (1999).
29. Hadzibabic, Z., Krüger, P., Cheneau, M., Battelier, B. & Dalibard, J. Berezinskii-Kosterlitz-Thouless crossover in a trapped atomic gas. *Nature* **441,** 1118–1121 (2006).
30. Lagoudakis, K. G. *et al.* Quantized vortices in an exciton–polariton condensate. *Nature Phys.* **4,** 706–710 (2008).

Supplementary Information is linked to the online version of the paper at www.nature.com/nature.

Acknowledgements We thank L. Levitov, T. Ostatnický, L. Sham, B. Simons and C. Wu for discussions. This work was supported by the DOE Office of Basic Energy Sciences (DE-FG02-07ER46449). The development of spectroscopy in a dilution refrigerator was supported by ARO and NSF. M.M.F. was supported by the UCOP. A.V.K. was supported by the Royal Society (UK).

Author Contributions All authors contributed to the work presented in this paper.

Author Information Reprints and permissions information is available at www.nature.com/reprints. The authors declare no competing financial interests. Readers are welcome to comment on the online version of this article at www.nature.com/nature. Correspondence and requests for materials should be addressed to A.A.H. (alex.high@gmail.com).